Closed-Loop Charged Relative Motion Experiments Simulating Constrained Orbital Motion

Carl R. Seubert and Hanspeter Schaub
University of Colorado, Boulder, Co, 80309

Simulated Reprint from

Journal of Guidance, Navigation and Control

Volume 33, Number 6, Nov.–Dec., 2010, Pages 1856–1865

A publication of the
American Institute of Aeronautics and Astronautics, Inc.
1801 Alexander Bell Drive, Suite 500
Reston, VA 22091

JOURNAL OF GUIDANCE, NAVIGATION AND CONTROL
Vol. 24, No. 1, Jan.–Feb., 2001

Closed-Loop Charged Relative Motion Experiments Simulating Constrained Orbital Motion

Carl R. Seubert* and Hanspeter Schaub†
University of Colorado, Boulder, Co, 80309

Coulomb spacecraft actively control their potential through continuous charge emission, generating inter-spacecraft electrostatic forces for formation control. This paper presents experimental results of autonomous relative motion control with Coulomb forces. Tests are performed in a terrestrial environment without resorting to expensive vacuum or plasma chambers. A simple charge feedback control algorithm is successfully implemented, yielding the first experimental closed-loop charged relative motion results. The results demonstrate how the one-dimensional test track mimics the constrained spacecraft orbital motion along the orbit radial, along-track, or out-of-plane directions. These dynamical systems are replicated by either leveling the test track or adding a small tilt to bias the relative motion in one direction. The relative motion is controlled by the dominant Coulomb forces even in the presence of induced bias and unknown perturbations. This paper quantifies primary disturbances and highlights the suitability of the vacuum force model to atmospheric force generation.

I. Introduction

The use of spacecraft formations for remote sensing, interferometry, and telescopic operations is a growing area of research where baselines of tens to hundreds of meters are sought to increase observation power and sensor resolution. Spacecraft formations can be used for scientific, surveillance or exploratory missions and offer advantages that include the use of smaller and lighter spacecraft, system redundancy, and distributed network space systems. The technical and logistical challenges of formation flight are being overcome with numerous successful missions and many concepts in planning.[1,2]

Close spacecraft formations on the order of dozens of meters present particular mission challenges including the need for very accurate relative position sensing, as well as frequent micro-Newton-level relative motion control maneuvers. The use of electrostatic (Coulomb) forces to control the relative position of close proximity spacecraft is an emerging concept that addresses these challenges. It offers precise and adjustable forces to control the complex relative dynamics.[3,4] Using conventional inertial thrusters such as chemical or electric propulsion at these close separation distances can introduce exhaust plume contamination. The Coulomb thrust technique avoids these close proximity plume impingement concerns. An example of a simple two spacecraft formation using Coulomb forces for separation distance control is shown in Figure 1.

Orbital missions such as SCATHA and ATS-6 have shown that spacecraft charging naturally occurs through interaction with the local plasma environment.[5,6] A spacecraft in Geosynchronous Earth Orbit (GEO) can naturally charge to kilovolt level potentials.[7,8] Natural spacecraft charging can be safely handled and overcome as shown with missions such as Equator-S, CLUSTER and SPEAR 1.[9,10,11] The European Space Agency (ESA) CLUSTER spacecraft maintain very precise potentials by emitting indium ions from a liquid metal source.[11] The Coulomb thrust concept described in this paper would ultimately employ space-proven technology such as this. Furthermore, it is the absolute potential of the craft that produces the Coulomb force, so natural charge levels can be utilized and then modified as necessary to perform an operational maneuver.

A primary feature of Coulomb thrust is that it offers precise separation distance control for very low power consumption (Watt levels) and very low propellant mass (ejects electrons or low-mass ions) making it significantly more efficient than conventional propulsion methods.[12,3] Due to the natural charge shielding effect from the space plasma environment it is most favorable to use Coulomb control with separation distances less than 100 meters and formation altitudes at high or geosynchronous orbits.[3]

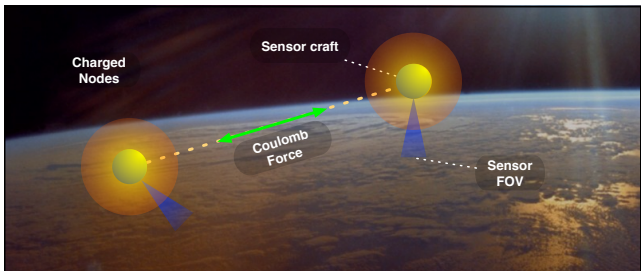

Figure 1: Two sensor nodes using Coulomb forces for formation separation distance control

Two future missions that could adopt Coulomb thrust techniques for formation control are the proposed NASA Goddard Stellar Imager[13] and the NASA JPL study on the proposed Terrestrial Planet Finder.[14] Terrestrial testbeds have been developed to explore the control techniques of spacecraft formations such as these. These include JPL's Formation Control Testbed[15] and NASA Marshall Space Flight Center flat floor testbed.[16] These testbeds provide flat, near frictionless operating surface that allow terrestrial relative motion experiments using air-bearing pads.

Attitude and relative motion experiments conducted on traditional testbeds are typically performed with systems with well-known dynamics and use actuators with force magnitudes much greater than the Coulomb thrust technique (micro- to milli-Newton level). A fundamental step to fully develop and implement the Coulomb thrust concept is the ability to perform relative motion experiments. Challenges that must be overcome to perform terrestrial environment experiments include; significantly small disturbance forces (< 1 mN), limited models of terrestrial charged forces in an atmospheric environment, the use of non-conducting and electrostatic-inert materials, and the safe control and operation of electrostatic potential sources. To address these challenges a dedicated Coulomb control testbed is being developed and tested.

The primary intent of the charged relative motion testbed is to explore the intricacies of utilizing Coulomb thrust. Developing and implementing the testbeds charged hardware components provides abundant knowledge that is not obtainable with purely numeric studies. The goal is to analyze the complexities of autonomous charged motion control, including force generation, partial charge shielding in atmosphere, electrostatic field interactions, material

*Graduate Research Assistant, Aerospace Engineering Sciences Department, University of Colorado, Boulder, CO. AIAA student member.
†Associate Professor, Aerospace Engineering Sciences Department, University of Colorado, Boulder, CO. AIAA Associate Fellow.
Presented as Paper 06–3792 at the AIAA Guidance, Navigation and Control Conference, San Diego, CA, July 29–31, 1996.

and shape studies, surface charge distribution, and arcing. The testbed also allows testing of charge feedback control strategies, and development of embedded electronics and inter-craft communication with vehicles that can accommodate variable ground levels. These are just some of the concept implementation aspects that can commence to be addressed with the Coulomb testbed.

This paper experimentally quantifies the significant reductions in the testbeds disturbance forces. Reduced disturbance levels enables the first closed-loop electrostatic feedback relative motion control tests to be performed on the one dimensional (1-D) track. The results of three test configurations inspired from the charged relative motion dynamics of two bodies along the principal orbit frame axes are presented. This is not an exhaustive study or an application of a refined control algorithm, rather the first demonstration of Coulomb relative motion control. The experiments verify how a simple control strategy can be used to reposition the floating body to desired positions in the presence of small disturbances and intentional force biases.

II. Coulomb Force

A Coulomb force is generated from the electrostatic interaction of two charged bodies. In a vacuum the force magnitude between two bodies of charges q_1 and q_2 is computed as:

$$|\boldsymbol{F}| = k_c \frac{|q_1 q_2|}{r^2} \tag{1}$$

where $k_c = 8.99 \times 10^9 \ \mathrm{Nm^2C^{-2}}$ is the vacuum Coulomb constant and r is the separation distance between the bodies. If the body is a spacecraft comprised of an outer spherical surface maintaining a constant charge the resulting potential in a vacuum is:

$$\Phi_1 = \frac{q_1 k_c}{\rho} \tag{2}$$

where ρ is the radius of the spherical craft.

In space, the Coulomb force is reduced (shielded) by free-flying charged particles of the local plasma environment. The strength of this shielding is parametrized by the Debye length λ_d.[17] Assuming a small craft potential compared to the local plasma thermal energy ($e_c\Phi_1 \ll \kappa T_e$, where $e_c = 1.602176 \times 10^{-19}$ C is the elementary charge, $\kappa = 1.38065 \times 10^{-23}$ JK^{-1} is the Boltzmann constant and T_e is the plasma electron temperature in Kelvin), the potential about this charged craft is represented by the Debye-Hückel equation:[18,19]

$$\Phi = k_c \frac{q_1}{r} e^{-(r-\rho)/\lambda_D} \tag{3}$$

where r is the distance from the spherical craft which has a finite radius ρ. Taking the gradient of this potential (assuming spherical symmetry) the resulting Coulomb force $\boldsymbol{F}_c$ between two charged craft with a separation distance r can be approximated by:

$$\boldsymbol{F}_c = q_2 \boldsymbol{E} = q_2(-\nabla\Phi) = k_c \frac{q_1 q_2}{r^2} e^{-r/\lambda_d} \left(1 + \frac{r}{\lambda_d}\right) \hat{r} \tag{4}$$

The Debye length is based on the temperature and density of the local plasma. At GEO the plasma is sufficiently hot and sparse to generate Debye lengths ranging from 80–1000 m with an average of approximately 200 m,[3,12] allowing the use of Coulomb thrusting when operating with spacecraft separations of dozens of meters at GEO. Low Earth Orbit (LEO) Debye lengths are typically on the order of centimeters, making the use of Coulomb thrust challenging for free-flying charged LEO objects.

To model the Coulomb force in the non-charged air (absence of charged particles) of the laboratory the Coulomb constant k_c in Equation 1 is adjusted to account for the relative permittivity of air. Measurements made of the true potential fields around spherical charged objects in the laboratory show discrepancies from predicted theory as well as additional differences between positive and negative potentials. The conclusion drawn is that there is a small interaction of the charged spheres with the local laboratory atmosphere and surrounding apparatus. The resulting reduced potentials (partial charge shielding) may be similar to the charge shielding a spacecraft experiences from its local plasma environment. These interactions are not discussed here, but future work will investigate and improve the accuracy of the atmospheric Coulomb force model by modifying Equation (1). In addition, Equation (1) assumes the nodes are modeled as spheres with an evenly distributed charge that sums to a total charge q_i. In reality, if the separation is within a few craft radii, the nodes will have induced charge which distributes the charge unevenly across the surface. For this paper and its intended scope the simple electrostatic relationship in Equation (1) is used in the analytical dynamic and control development and is used simply as a benchmark for experimental results. The presented tests allow for future experiments to verify any induced charge models.

III. Testbed Hardware Apparatus

The Coulomb testbed in the Autonomous Vehicle Systems (AVS) laboratory at the University of Colorado at Boulder is developed specifically to autonomously control vehicles with Coulomb forces. The testbed design and preliminary experiments demonstrating electrostatic actuation on the track is described in detail in Reference.[20] The disturbances in these results were still rather large (on the order of 10s of milli-Newton). The testbed has received modifications and improvements to reach its present state which is used to obtain the results presented in this paper.

The unique and cost-effective custom testbed is shown in Figure 2. It features chargeable spheres with one on a cart that moves along a near-frictionless air bearing track. The vehicle's position is manipulated by controlling the charge level of the spheres which is driven by their respective potential levels as modeled with Equation 2. Future testbed generations will evolve to two dimensions and ultimately incorporate vacuum operation and environmental modeling.

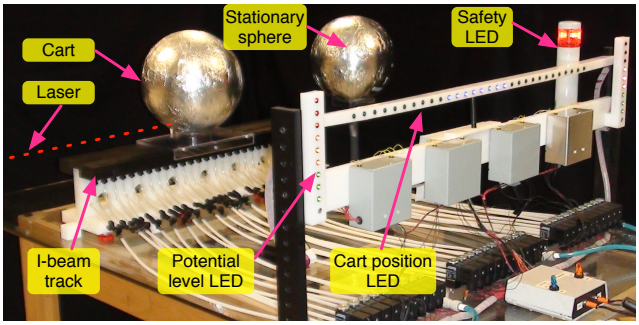

Figure 2: Testbed for 1-D cart position control with Coulomb forces

As shown in Figure 2, the testbed comprises an all plastic 1-D air bearing track. It features an autonomous air flow system using infrared (IR) sensors and valves to control the air to flow only underneath the cart. Polarity switching electrostatic power supplies, capable of $\pm$30 kV, are used to charge the aluminum spheres and control the motion of the cart. Each sphere has a diameter of 25 cm, while the total cart mass is 0.5 kg. The sphere size is chosen to maximize charge, minimize mass, and allow an adequate range of motion on the track length. The sphere's are wrapped in aluminum to give a conducting surface. This aluminum surface provides an equivalent Coulomb force level as polished stainless steel while providing significant mass savings. An Acuity laser range finder with sub-millimeter accuracy is used for external position sensing. The laser range finder signal is sampled at 50 Hz. Statistical measurements of the accuracy of each of these commercially available products is shown in Table 1.

The entire apparatus sits on a glass table, a strong non-conductor, to limit external charge interference. The table is positioned inside a plastic cage for operational safety and is always operated with two personnel. The testbed also implements LED warning systems indicating sphere potential levels and cart position.

A feedback control algorithm is implemented with the testbed hardware through a custom C-code application. A schematic of the primary hardware systems and feedback loop is shown in Figure 3. A custom graphical user interface (GUI) allows the user to run the

Table 1: Statistical measure of the accuracy of laser and power supplies

Measurement:	Standard deviation (3-σ)
Laser measurement	< 0.05 cm
Rated voltage output	0.003 kV
Analog measurement of voltage	≈ 0.4 kV

autonomous control scheme as well as any of the hardware systems manually and independently.

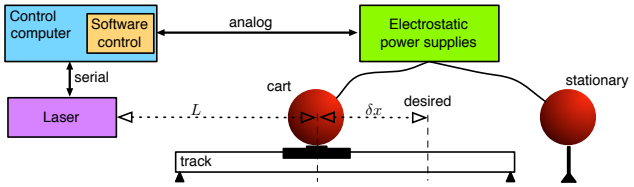

Figure 3: Schematic of testbed primary hardware systems and feedback implementation

The track length currently used is 0.5 meters long. This length allows for interesting electrostatic station-keeping experiments to be performed. The setup is general enough to allow multiple-craft to levitate on the track. Using only one cart on the track allows relative position control experiments where non-zero equilibrium charges must be generated if the track is slightly tilted, simulating a gravity bias in the relative motion.

IV. Disturbances

One of the greatest challenges to overcome with the Coulomb testbed is the mitigation of small disturbances. It is necessary to reduce disturbances to levels less than the electrostatic forces, allowing the relative motion dynamics to be dominated by the Coulomb forces. With a nominal stationary sphere location, the range of Coulomb control force achievable is 3-18 mN with both repulsion and attraction. To maintain a signal-to-noise ratio (Coulomb : disturbances) greater than one and providing an additional margin, it is desirable to reduce all disturbance forces to below 2 mN. In this section, sources of disturbances are highlighted and methods of reduction presented.

To measure the extent of track disturbances simple glide test are performed. Here the cart is given a small impulse at one end of the track and ideally glides with constant velocity to the other end of the track. The first test results discussed in Reference[20] showed disturbance forces over 10 milli-Newton in magnitude. While small, this limited previous experiments to be performed in sub-sections of the track at close separations where Coulomb forces dominated.

Modifications to the current testbed track such as regularization of the airflow and obtaining a level track have greatly reduced gravitational and flow disturbances. Further, a new cart is manufactured from polycarbonate for its smooth surface, dimensional stability and resistance to conduct and hold charge.

Another important consideration with the Coulomb testbed is maneuver durations. For GEO spacecraft clusters the maneuvers can last for fractions of days, to multiple days, and the differential disturbance forces are 1-2 orders of magnitude smaller than the Coulomb forces.[21] In the laboratory, differential perturbations are a similar order of magnitude to the Coulomb control force. To accommodate this, it is necessary to maximise the electrostatic charges to create milli-Newton level forces, compared to the more typical micro-Newton level forces in space. As a result, the maneuver times are reduced for the laboratory experiments to the order of minutes instead of hours.

A. Gravitational Disturbances

Gravitational accelerations are reduced through improved track surface smoothness and leveling. The first generation of plastic tracks warped as much as 0.1° which equates to a disturbance force as great as 8.5 mN. A 2 mN gravity disturbance corresponds to a track angled at 0.024°. Resurfacing of the track in its constructed I-beam design in a unstressed state reduced the total height variation along the track length of 0.5 meters to below 0.1 mm. The resulting worst case local deviation occurs at only one end of the track which has a maximum angle deflection of 0.02° (≈ 1.7 mN), which is better than desired. An additional gravitational disturbance can occur from uneven mass distribution of the cart. The cart is precisely mass balanced and verified with glide tests prior to Coulomb testing, however this is another potential source of modeling error.

B. Glide Test Disturbances

The disturbance forces acting on the cart during glide tests are evident in Figures 4 and 5. These figures show the cart's speed profile for a number of tests without Coulomb forces applied. The tests are conducted over a very flat and level 35 cm track section with varying initial impulse speeds. Figure 4 shows the speed of the cart as it moves toward the stationary sphere as a function of track location, while Figure 5 shows the speed profile traveling in the opposite direction.

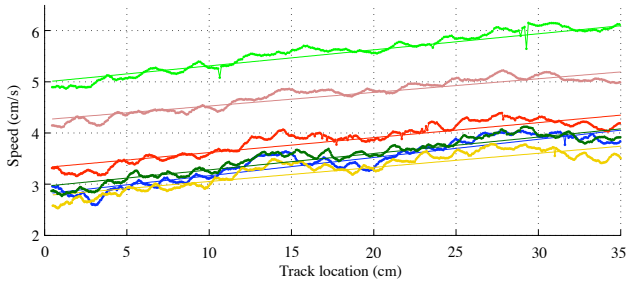

Figure 4: Cart glide data toward stationary sphere

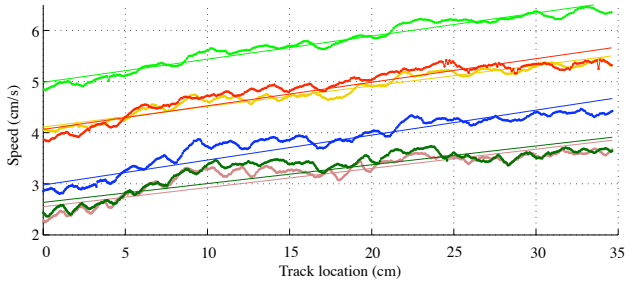

Figure 5: Cart glide data away from stationary sphere

The data shown in Figures 4 and 5 indicates a disturbance acceleration acting on the cart in both directions of travel. The average force acting on the cart during these glide tests is computed by taking the derivative of the position measurements. For this 0.5 kg cart the average force is calculated to be approximately 1.0 mN when traveling toward the stationary sphere in Figure 4 and approximately 0.9 mN when traveling away in Figure 5. The acceleration is near uniform across all initial speeds for both data sets.

The primary cause for the cart accelerating in both directions is believed to be a slight cart tilt due to uneven air-support as it moves between rows of air holes. This small acceleration is only present if the cart is moving to begin with. These glide tests are used to ensure the overall track surface is level prior to electrostatic actuation tests.

The intent of plotting the speed profile as a function of track location is to highlight any common disturbances. In some track locations there are small deviations across all speeds and both directions indicating localized discrepancies in track surface and air flows. These slight disturbances represent what is present on the testbed for the Coulomb test results shown in this paper. During these experiments the controlling Coulomb force repeatedly dominates these small disturbance forces.

To further identify disturbance sources a spectral analysis of the force data is conducted. The data from the glide tests in Figure 4 is differentiated with a low pass filter below 10 Hz to obtain the acceleration. The data is de-trended to remove the linear acceleration. Figure 6 shows the equivalent magnitude of the force oscillations occurring at any particular frequency. There is a distinct 0.3 mN magnitude peak at $\approx$ 1.8 Hz. This peak corresponds to a natural oscillation in the raw laser position data. It is the next largest disturbance during glide tests (behind the constant acceleration term) and is an order of magnitude lower than the desired minimum disturbance level. The position accuracy of the laser enveloping this small 1.8 Hz oscillation is given in Table 1. Overall, this indicates that the system has minimal external disturbances during gliding, with no distinct cart wobble or low frequency interference.

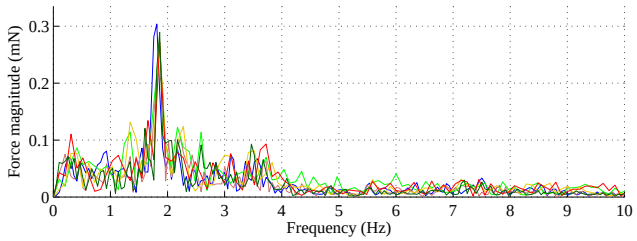

Figure 6: Spectral analysis of glide test data showing magnitude of force oscillations

C. Air Flow Disturbances

Figures 4 and 5 are used to isolate local track position disturbances. Total air pressure is minimized and uneven airflows from each row of holes is accurately monitored and regulated to reduced undesired torques on the cart. To study and mitigate the effects of inaccurate cart positioning and the triggering of airflow, numerous glide tests are conducted with the cart prior to all Coulomb control experiments to ensure a minimum disturbance state is reached. An optimum configuration of minimum disturbance is used for all Coulomb experiments conducted and presented in this paper.

D. Electrostatic Disturbances

The testbed is designed to minimize electrostatic interference and the effects of induced charge, however, these disturbances are present. Evaluating the extent of these disturbances is not trivial and is the intent of future studies. As the results demonstrate, the controlling Coulomb forces overcome these perturbations.

V. Constrained Relative Motion Dynamics and Control

Theoretical studies based on the Coulomb thrust concept is a growing research area. Berryman and Schaub investigate the use of Coulomb control to create static equilibrium configurations in orbit.[22,23] This includes analytic two- and three-craft charged relative equilibria in a rotating Hill frame.[22] This was later expanded to three dimensions with four-craft relative equilibria.[24] For the two-craft system, the linear orientation can be paralleled to the charge control motion being achieved on the 1-D testbed.

While relative equilibrium solutions for Coulomb spacecraft clusters have been developed, all these open-loop equilibria are naturally unstable. To implement a two-craft virtual Coulomb structure concept it is necessary to introduce feedback control. Reference[21] develops a control that stabilizes the motion of two craft about an orbit radial alignment while maintaining a fixed separation distance. Reference[25] details a restricted 1-D Lyapunov-based Coulomb control regime developed for three craft operating in a linear configuration. Reference[26] further develops the 1-D constrained control techniques to analyze the feasible regions of operation that can be implemented ensuring that the charge levels are realistic and do not saturate, both important considerations for hardware implementation. The ultimate goal of the testbed is to directly apply and study closed-loop charge control algorithms such as these on Coulomb actuated hardware. The real-time feedback control experimental results presented here are similar to 1-D constrained orbital motion in orbit radial, along-track and out-of-plane directions.

A. Testbed Dynamics

The terminology used in the testbed control algorithm is defined in Figure 7. The laser measures the distance to the cart L, which corresponds to the distance x from the stationary charged sphere. The desired position of the cart x_r defines the tracking error $\delta x = x - x_r$.

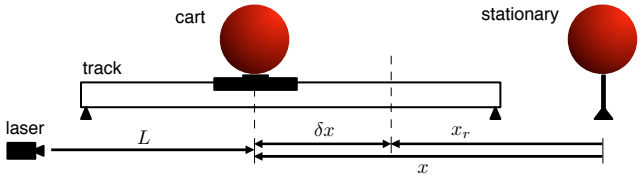

Figure 7: The testbed variable definitions

Using the Coulomb force in Equation (1), the equation of motion for the cart on the track is defined by:

$$\ddot{x} = f(x,u,t) = \frac{1}{m}\left[\frac{k_c Q}{x^2} + f_{\text{system}} + f_{\text{unknown}}\right] \tag{5}$$

where $Q = q_1 q_2$ is the combined charge product, f_{system} represents known forces acting on the system (such as intentional gravity biases) and f_{unknown} are unmodeled disturbance forces. The cart motion control parameter is the combined charge product Q.

B. Constrained 1-D Charged Relative-Orbit Dynamics

The intent of the testbed and associated control methodology is not to simulate actual relative orbit dynamics. Rather, restricted 1-D relative motions are of interest. It is possible for the testbed to mimic 1-D constrained orbital relative motion along a principal orbit frame axis. To develop the relative equations of motion, the rotating Hill frame $\{\hat{o}_r, \hat{o}_\theta, \hat{o}_h\}$ with its axes aligned with the orbit radial, along-track and out-of-plane directions respectively is used. The spacecraft position $\boldsymbol{\rho}_i$ is expressed in this Hill frame with Cartesian $\{x, y, z\}$ coordinates. Figure 8 illustrates both the rotating Hill frame, as well as the three possible 2-craft charged relative equilibrium configurations aligned with the orbit radial, along-track and out-of-plane axes.

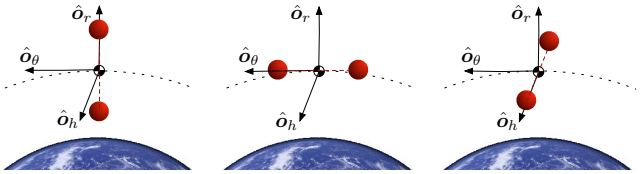

Figure 8: Two spacecraft example of the orbit radial, along-track and out-of-plane charged relative equilibrium operating configurations in the rotating Hill frame

Equations (6) show the linearized Clohessy-Wiltshire-Hill (CWH) equations subject to electrostatic actuation in a plasma environment.[21] The CWH equations define the motion of a satellite relative to the circularly orbiting Hill frame. With a formation of N Coulomb controlled spacecraft the CWH equations of the i^{th} spacecraft relative to the orbit reference is defined by:[21]

$$\ddot{x}_i - 2\Omega\dot{y}_i - 3\Omega^2 x_i = \frac{k_c}{m_i}\sum_{j=1,j\neq i}^{N}\frac{(x_i - x_j)}{|\boldsymbol{\rho}_i - \boldsymbol{\rho}_j|^3} q_i q_j e^{-r_{ij}/\lambda_d}\left(1 + \frac{r_{ij}}{\lambda_d}\right) \tag{6a}$$

$$\ddot{y}_i + 2\Omega\dot{x}_i = \frac{k_c}{m_i}\sum_{j=1,j\neq i}^{N}\frac{(y_i - y_j)}{|\boldsymbol{\rho}_i - \boldsymbol{\rho}_j|^3} q_i q_j e^{-r_{ij}/\lambda_d}\left(1 + \frac{r_{ij}}{\lambda_d}\right) \tag{6b}$$

$$\ddot{z}_i + \Omega^2 z_i = \frac{k_c}{m_i}\sum_{j=1,j\neq i}^{N}\frac{(z_i - z_j)}{|\boldsymbol{\rho}_i - \boldsymbol{\rho}_j|^3} q_i q_j e^{-r_{ij}/\lambda_d}\left(1 + \frac{r_{ij}}{\lambda_d}\right) \tag{6c}$$

where m_i is each spacecraft's mass and the system center of mass has an orbital rate $\Omega = \sqrt{\mu/R_c^3}$ with R_c being the orbit radius and μ the gravitational constant. These equations are constrained to 1-D motion along the orbit radial, along-track and out-of-plane directions and compared to possible testbed 1-D motions. To maintain a two-node static formation it is necessary for the center of mass of the system to be located at the origin of the Hill frame. With only two craft in the formation and ignoring any plasma Debye shielding, the 1-D relative equations of motion become:

$$\ddot{x}_i - 3\Omega^2 x_i = \frac{k_c}{m_i}\frac{(x_i - x_j)}{|x_i - x_j|^3}Q \tag{7a}$$

$$\ddot{y}_i = \frac{k_c}{m_i}\frac{(y_i - y_j)}{|y_i - y_j|^3}Q \tag{7b}$$

$$\ddot{z}_i + \Omega^2 z_i = \frac{k_c}{m_i}\frac{(z_i - z_j)}{|z_i - z_j|^3}Q \tag{7c}$$

where $Q = q_i q_j$ is the combined charge product. Equation (7a) represents the restricted 1-D orbit radial relative motion. This equation is the form of an unstable oscillator meaning the spacecraft will naturally drift apart due to the gravity gradient, expressed by the $(-3\Omega^2 x_i)$ term. However an equilibrium condition is reached (x_i held constant) if an attractive Coulomb force is applied. This equilibrium is achieved with a heterogeneous charge product solution:[22]

$$Q = -3\Omega^2 x_i \frac{m_i|x_i - x_j|^3}{k_c(x_i - x_j)} < 0 \tag{8}$$

This charge product solution requires each vehicle to have an opposing charge polarity. To mimic this operating scenario on the testbed, the track is intentionally tilted so a gravity bias force naturally repulses the cart from the stationary sphere. Attractive Coulomb control (Q) is used to drive and hold the cart at a desired separation distance.

Similarly, Equation (7c) represents the restricted 1-D out-of-plane relative motion, assuming no perturbations. The spacecraft will naturally drift together due to the gravity gradient, expressed by the $(+\Omega^2 z_i)$ term. However an equilibrium condition is reached (z_i held constant) if a repulsive Coulomb force is applied. This equilibrium is achieved with a homogeneous charge product solution:[22]

$$Q = \Omega^2 z_i \frac{m_i|z_i - z_j|^3}{k_c(z_i - z_j)} > 0 \tag{9}$$

This charge product solution requires each vehicle to have the same charge polarity. This configuration is comparable to experiments on the testbed with an intentionally inclined track providing a constant gravity bias force naturally attracting the cart to the stationary sphere. Repulsive Coulomb control (Q) is used to drive and hold the cart at a desired separation distance.

Note that these two inclined track setups do not match the constrained relative orbit motion precisely. The test track has a constant acceleration bias, while the orbit motion is a position dependent bias. However, both setups result in the nominal charge product Q being nonzero once the craft reaches the desired equilibrium state.

Equation (7b) represents the restricted 1-D along-track relative motion that is inherently stable without perturbations. To maintain equilibrium (y_i constant) requires no charge, $Q = 0$. This condition is simulated on the testbed with a level track and no bias accelerations. Of these three simulations, the along-track direction is the most challenging to implement because of the need to have a flat and level track. Even small residual disturbances can move the cart once it reaches its desired location. The orbit radial and normal direction simulations are easier to implement since any track un-level biases can be exploited to provide slight gravitational pull or repulsion to simulate this charged axial orbital motion. Here the small disturbances are over-shadowed by the larger intentional gravity bias of the track tilt.

To put these 1-D dynamic analyses into perspective, consider an example two-craft system operating in a radial configuration in GEO. The radial differential gravity force magnitude linearizes to:[12]

$$\delta F_r \approx m\frac{3\mu}{R_c^3}r \tag{10}$$

where m is the spacecraft mass and r is the spacecraft separation distance. Consider two craft of 50 kg mass each, aligned in the radial direction with a separation of 20 m. At GEO the craft experience a repulsive gravity gradient force of approximately 16 μN. To overcome this force with Coulomb thrust requires a heterogenous charge of $Q \approx -0.71$ pC calculated using Equation (4) with a plasma Debye length of 200 m. This charge corresponds to a required voltage magnitude of approximately 15.2 kV, calculated using Equation (2) with a spherical craft of 0.5 m radius.

Similarly, consider the same two spacecraft operating in an out-of-plane configuration at GEO. The differential out-of-plane gravitational force magnitude linearizes to:[12]

$$\delta F_h \approx m\frac{\mu}{R_c^3}r \tag{11}$$

With a 20 m separation the attractive force is approximately 5.3 μN. To overcome this force with Coulomb control requires a homogenous charge of $Q \approx 0.24$ pC, corresponding to a spacecraft voltage magnitude of 8.8 kV.

C. Testbed Charge Feedback Control Law

A goal of this paper is to demonstrate stable position feedback control actuated with Coulomb forces. A PID controller is implemented to stabilize the cart motion about a desired fixed track location. There is no benefit in developing a further refined control law at this stage, as the system model requires further enhancements to include complex electrostatic effects such as close proximity induced charges. This controller suitably accounts for the unmodeled disturbance forces and introduces system damping which is not inherent to the testbed. A feedback linearizing control solution is chosen of the form:

$$Q = \frac{x^2}{k_c}\Big(- k_D\delta\dot{x} - k_P\delta x - k_I\int_0^t \delta x dt - f_{\text{system}}\Big) \tag{12}$$

where k_P, k_D, and k_I are positive constant controller gains, and $\delta x = x - x_{\text{r}}$ is the tracking error with respect to a constant reference position x_{r}. This non-linear charge feedback control law Q features feed-forward compensation when known biases f_{system} are acting on the hovering cart. The integral feedback component adds robustness to the steady state system response accounting for discrepancies in the modeling of f_{system} and the limited model of charge interaction with the atmosphere. Future modeling of electrostatic disturbances could be added to this control law. Substituting the control law Q into the equation of motion in Equation (5) results in the following closed-loop dynamics:

$$\delta\ddot{x} + k_D\delta\dot{x} + k_P\delta x + k_I\int_0^t \delta x dt = f_{\text{unknown}} \tag{13}$$

With positive control gain values the feedback linearized system response is stable assuming the un-modeled disturbance f_{unknown} is constant. Note that to implement the charge feedback control Q in Equation (12), it is still required to map Q into individual charges q_i. In the following numerical and experimental simulations the simple solution of $q_1 = -\sqrt{|Q|}$ and $q_2 = Q/q_1$ is used. This solution is chosen as it is easily implemented on the testbed. For spacecraft the value of q_i can be selected based on a weighting of quantitative parameters such as charge control power usage, charge saturation or equilibrium charge which are functions of the local space plasma and operating conditions.

D. Numerical Closed-Loop Performance Simulation

System performance and gain selection of the controller is simulated prior to implementation on the testbed. The cart motion response is numerically simulated using the Coulomb charge control defined in Equation (12). For sloped track experiments mimicking

a 1-D relative orbit bias, a constant force of 1-3 mN is added to the model through the f_{system} term.

An example simulation is presented here as a baseline to demonstrate controller setup procedure and simulation prior to testbed experiments. It is not anticipated that the hardware implemented response will resemble this example performance due to discrepancies in the model. This simulation features a cart initially at rest with a sphere separation of 30 cm (center to center). The track is tilted downward from the stationary sphere inducing a constant repulsive gravity bias of 2 mN, producing similar dynamics to a radially aligned orbit configuration. The cart is then accelerated and controlled to a fixed position 30 cm downhill and held there with the Coulomb force. Table 2 lists the controller gains which are selected to give an underdamped response without saturation, an overshoot $< 15\%$ and a 5% settling time of 25 seconds. These values are used for the simulation as well as the proceeding experimental results. The resulting numerical simulation performance of this example is shown in Figure 9.

Table 2: Desired performance and control gains used for the example simulation

Overshoot:		$< 15\ \%$	
5% Settling time:		≈ 25 s	
Control gain:	k_D	k_P	k_I
Value:	1800	300	100

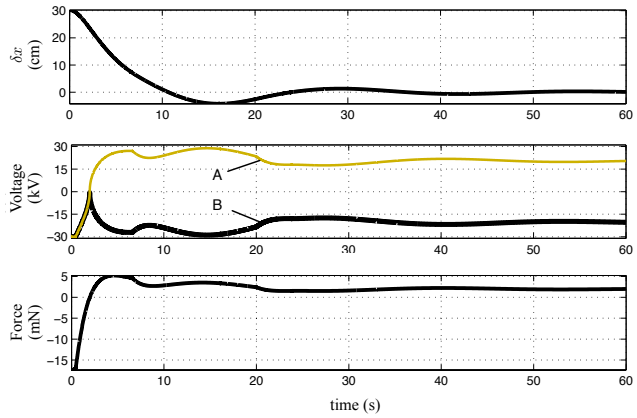

Figure 9: Simulation of cart motion with a constant system repulsive force of 2 mN

Figure 9(a) shows the distance of the cart away from the desired location in centimeters. The response of the cart has a 13% overshoot and a 5% settling time of 23 seconds. This is suitable for the control of the cart on the testbed and is controllable with feasible voltages as shown in Figure 9(b) where the cart voltage is shown with line (A), while the stationary sphere voltage is shown with line (B). As shown, initially the cart is repelled away with a homogeneous charge. But the voltage quickly changes to heterogeneous polarity, producing an attractive force that prevents the cart from sliding down the simulated sloped track. The steady state voltage shown in Figure 9(c), is $\approx$ 20 kV which provides a 2 mN force (calculated using Equation (1) and final separation distance).

Voltage saturation occurs only for the initial second, however around 15 seconds into the simulation the required voltages almost saturate again. Due to the controls low signal-to-noise actuation forces and the inclusion of a bias force here, there is a small margin between controllability and voltage saturation. This is something to be considered with space-based implementation where charge limitations are in place. Fortunately, space-based Coulomb actuation forces have a much larger signal-to-noise ratio. Control saturation is an undesired condition, however it does not prevent stable position control as shown in Reference.[27] Additionally, the simulation has no limit on the charge rate capabilities. In space it has been shown that active charge control devices can reduce the spacecraft charge from kilovolt levels within seconds for reasonable power levels.[28,11]

VI. Position Control Experimental Results

The results of four experiments are presented that demonstrate the relative motion of a Coulomb controlled cart on a flat and level track as well as an inclined track. The intent here is to implement Coulomb control and use inclined track experiments to mimic simplified out-of-plane (relative attractive acceleration) or orbit radial (relative repulsive acceleration) motions.

A. Configuration 1. Out-of-Plane: Starting Down Slope

The Coulomb control algorithm is first implemented on an intentionally inclined track that slopes upward away from the stationary sphere. The cart is initially at rest at a separation of 30 cm (center to center) from the stationary sphere and ascends the track under Coulomb force. Figure 10 displays both the simulation and experimental results of driving the cart a total of 12 cm up slope to a final separation of 42 cm. The simulation has a 2.0 mN bias force added and the same control gains as the hardware.

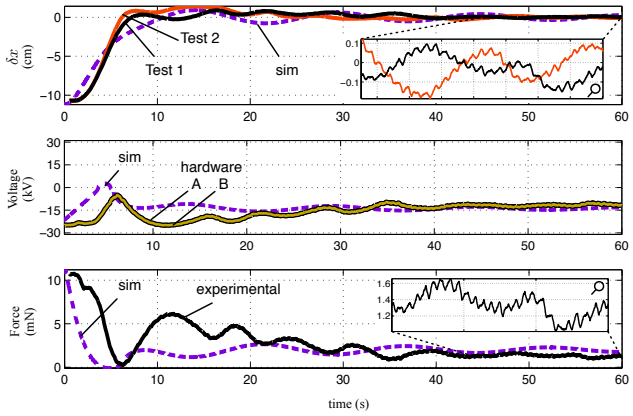

Figure 10: Inclined track cart control that mimics two craft in an out-of-plane orbit configuration (starts down slope), including simulated control performance

The cart tracking error δx is shown in Figure 10a for two identical tests. A magnification showing the settlement of the cart at the desired location is also shown for each test. Two test sets are used for each experiment for consistency. Figure 10b shows the voltage levels that are used to control the cart during test 1 for both the cart sphere (A) and the stationary sphere (B). By design, the spheres are driven to negative potentials when repulsive forces are required. Figure 10c shows the Coulomb force acting on the cart in test 1 using the model defined in Equation (1).

The experimental and simulation results share similar characteristics. The system controlled response for both the simulation and experimental tests meet the nominal performance parameters outlined in Table 2. For the experimental results the cart has a 9.0% overshoot for test 1 and 13.6% for test 2, a 5% settling time of $\approx$ 23 s, and settles to $\pm$ 1 mm of the desired location. The simulation has a 10% overshoot and a 5% settling time of 25 s. The charge required to drive the cart this distance and hold the position on the inclined track remains a constant homogeneous charge (repulsive force). The resulting voltage to maintain the cart at this location is measured to be $\approx -12kV$ which equates to a force of $\approx$ 1.4 mN, calculated using Equation (1), whereas the simulation force is 2.0 mN. Using glide test data collected after these out-of-plane experiments it is found that the acceleration acting on the cart at this location equates to $\approx$ 2 mN.

While the overall simulation and experimental cart motions are similar there are some observations to note. There is a delay in the acceleration of the experimental cart perhaps due to charge build up time. Small discrepancies between simulation and experimental results are evident with the required voltage which peaks earlier for the simulation and requires a small period of heterogenous charge.

Correspondingly the simulation force peaks earlier, indicating a delay in the true system response.

At steady state the sub-millimeter, 1.8 Hz oscillations from the laser are evident. The longer period oscillations are the controller actuated response of the cart settling to its desired location. These attributes are present in all of the experimental results.

As voltage saturation occurs for the remaining three experimental configurations the response is not directly compared to the corresponding simulations results. The experimental results demonstrate Coulomb control and provide insight into the actuation capabilities.

B. Configuration 2. Out-of-Plane: Starting Up Slope

A second out-of-plane test starts with the cart at rest up slope that then descends to the desired position. The cart is initially separated by 72 and 65 cm (center to center) and driven down slope to a separation of 42 cm from the stationary. As shown in Figure 11, there is a large overshoot of 33% for test 1 and 48% test 2. In both tests the cart is moved to within ± 2 mm of desired. The 5 % settling time is 24 s for test 1 and 28 s for test 2. The steady state voltage is ≈ -15 kV which equates to a force of ≈ 2.2 mN, calculated using Equation (1).

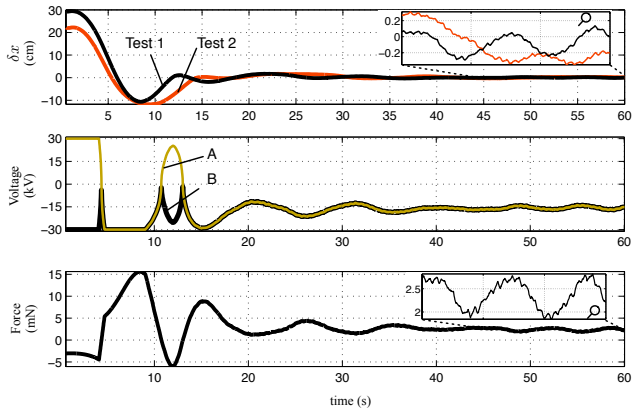

Figure 11: Inclined track cart control that mimics two craft in a out-of-plane configuration (starts up slope)

An important outcome of this experiment is the resulting voltage saturation. Simulations do not predict saturation, so this outcome in the experimental application confirms that the control force is reduced from the baseline Equation (1) relationship.

C. Configuration 3. Orbit Radial

This test configuration intentionally inclines the track sloping down from the stationary sphere. Figure 12 displays the results of controlling the cart a total of 28 cm down slope. The cart starts from rest and repels from an initial separation of 30 cm (center to center) from the stationary sphere.

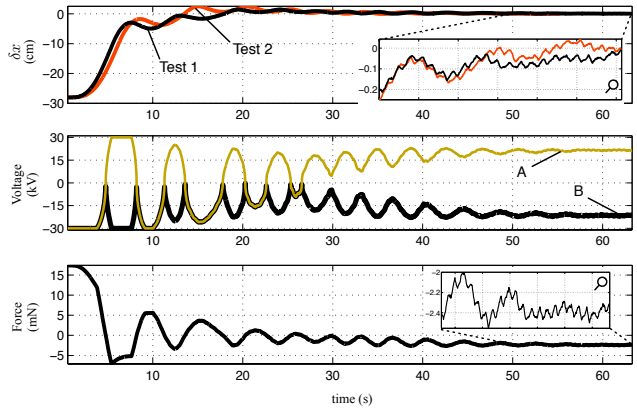

Figure 12: Inclined track cart control that mimics two craft in a orbit radial configuration

The system controlled response meets the nominal performance parameters outlined in Table 2. The cart has a 5.3% overshoot for test 1 and 8.9% for test 2. There is a 5% settling time of ≈ 25 s with a 1% settling time of 43 s for test 1 and 47 s for test 2. The cart is within 1 mm of the desired location within 55 seconds for each test. The craft is held at this fixed separation distance on the inclined track by holding a constant heterogeneous charge (attractive force).

The voltage levels required to drive the cart to rest show a steady state voltage of $\pm$ 21.5 kV. The steady state Coulomb force shown in Figure 12(c) indicates an attraction of ≈ 2.4 mN at this separation distance. With the voltage removed the cart accelerates away from the stationary sphere. Glide tests performed immediately after the Coulomb tests indicate the acceleration from this location to be ≈ 4.5 mN.

D. Configuration 4. Along-Track

For this experimental configuration the track is leveled using both precision level instruments and verified via glide test with the cart. Figure 13 displays the cart motion as it is driven a total distance of 30 cm from rest at an initial separation of 30 cm (center to center) from the stationary sphere.

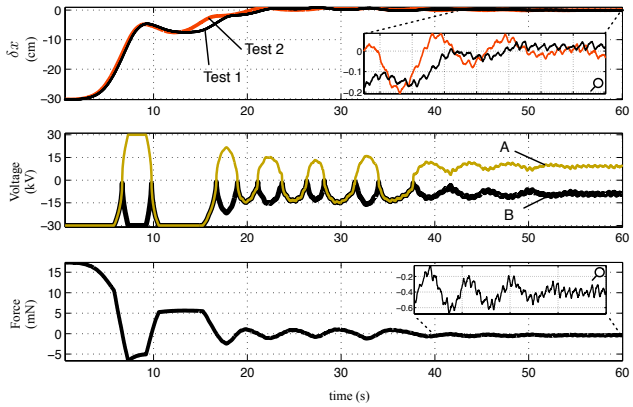

Figure 13: Flat and level track cart control that mimics two craft in an along-track orbit configuration

The system controlled response meets the nominal performance parameters outlined in Table 2. The system has a 3.3% overshoot for each test and a 5% settling time of 19 s and a 1% settling time of 34 s for test 2 and 39 s for test 1. The cart is within 1 mm of the desired location within 45 seconds of the tests duration.

For a level track it is anticipated that the control voltage is zero, however the steady state voltage is $\pm$ 9 kV. At this separation distance the resulting attractive Coulomb force is ≈ 0.4 mN. The source of this disturbance force is being examined, however it is likely a result of electrostatic induced effects and interaction of the spheres with the atmospheric environment in the lab.

VII. Discussion

The primary outcome of these experimental results is the successful implementation of autonomous relative motion control using Coulomb forces on an atmospheric testbed. The results offer some interesting findings that warrant discussion. Firstly, charge saturation is common to all test configurations. A saturated control authority is undesired, however the test cases still stabilize the cart motion. The conclusion drawn from this observation is that the Coulomb force produced on the testbed is reduced from the simple vacuum calculation of Equation (1).

The force discrepancy is also witnessed with a comparison of the simulation and experimental results of configuration 1 (out-of-plane). The resulting cart motion and steady state parameters are similar, but sustained higher voltage/force magnitudes are required to reach the desired location. In order to improve this controller a higher fidelity laboratory/atmospheric Coulomb force model is required.

It should be noted that while these experiments have similar dynamics to constrained 1-D orbital motion, they are not identical. Two significant deviations are the ratio between Coulomb actuation force levels relative to the disturbance forces. The applied constant

disturbance forces of the testbed are orders of magnitudes greater than what is anticipated in orbit. For this reason it is necessary to increase the time of maneuvers on the track allowing Coulomb forces to dominate.

A summary of the response characteristics of each test is displayed in Table 3. The 5% settling time indicates that for all test configurations the Coulomb force (even with saturation) successfully drives the cart to the desired position within the nominal time.

Analyzing the cart motion and percentage overshoot indicates there are different system responses depending on the charge characteristics used. Having a heterogenous charge (attractive Coulomb force) produces a heightened system response compared to a homogenous charge (repulsive force) at equivalent separations. This charge dependent response explains the undershooting that occurs in configurations 1,3, and 4 that initially require repulsion before switching to the increased attractive force. In these scenarios the system still manages to rebound and drive the cart to the desired location. Alternatively, configuration 2 (out-of-plane, starting up slope) commences with a heterogenous charge and the cart has a significant overshoot when switching to the lower control authority of the homogenous charge.

The likely cause of the different control authorities of homogenous and heterogenous charge products is due to uneven charge distribution at close proximities. Two closely separated spheres of opposing charge (heterogenous) have a higher force than the homogenous case as the surface charge is attracted to the closest separation of the spheres decreasing the apparent charge separation. Modeling this affect and implementing it into the control law is currently under investigation.

The affects of this induced charge is reiterated by inspecting the steady state position response of each configuration. Configurations 1 and 2 (out-of-plane) require a final homogenous charge and experience larger oscillations to reach the desired location. Adversely, the response of configurations 3 and 4 that result in heterogenous solutions settle earlier, because the force production is more consistent. In order to compensate for the lower control authority of the steady state homogenous charge solution the carts travel distance is reduced for configurations 1 and 2, decreasing the overall sphere separations and allowing the cart to come to a controllable rest.

Table 3 also presents the steady state results of each test configuration. The steady state voltage is measured from the power supplies while the steady state force is computed using Equation (1). The post-test glide force is computed from the average of speed vs time data with no electrostatics. Care has to be taken in comparing these force values. The Coulomb force model is limited and there are known sources of error both in the measurement devices (Table 1) and with the computation of the estimated gravity force (glide tests). Regardless, one reason for the discrepancy between steady state forces is electrostatic interferences. In particular, when the charge was removed on the flat and level configuration the cart remained stationary, suggesting that with the charge present it is in equilibrium with an induced electrostatic disturbance force.

Measuring the force discrepancy between charging methods and uneven distributions is difficult to quantify. It is a combination of the absolute and relative charge magnitudes, separation distance, track location, laboratory conditions and test durations. However, to really improve the control characteristics and system response it is necessary to further develop the Coulomb force model of the terrestrial testbed. This model improvement requires further testing and verification of the charge fields and apparatus interference, any shielding from the atmosphere, and induced charge effects at close separations, which is ultimately the intent of the testbed. For now, the feedback control is implemented on the hardware and Coulomb forces successfully perform relative motion control.

Future model improvements performed with estimation of the atmospheric/laboratory force actuation are beneficial to the Coulomb testbed experiments and extend to space-based applications. Using accurate relative range data measurements and known charge levels is a parallel between both the craft on the testbed and spacecraft modeling the local plasma conditions.

VIII. Conclusions

This paper presents the first charge feedback control experiments using a terrestrial Coulomb testbed. Experimental glide test results illustrate significant reductions in disturbance forces which consequently improves the Coulomb actuation capabilities of the testbed. A new and exciting feature, and major focus of this paper, is the implementation of a charged position feedback control. The results of position control on both a flat and level track as well as an inclined track are presented. These experiments are beneficial as they mimic the restricted 1-D motion that is experienced by two craft flying in a close orbit formation experiencing a gravity gradient force.

Significant theoretical and technical knowledge is gained from implementing Coulomb control on hardware as opposed to purely numerical studies. These successful autonomous position feedback control results open opportunities for future studies with the Coulomb testbed. The testbed allows hardware in the loop demonstrations of more advanced relative motion control algorithms. Known discrepancies in force models can be improved with further examination of electrostatic and environmental effects. These fundamental developments are also integral to space-based applications to ultimately advance the Coulomb thrust concept.

Acknowledgements

The authors would like to thank the invaluable contributions to this work by Nicolas Zinner, Eric Kenney, Steven Eskridge, Matt Rhode, Jill Tombasco, and the AVS lab group.

References

[1]J. Leitner, F. Bauer, J. How, M. Moreau, R. Carpenter, and D. Folta, "Formation Flight in Space: Distributed Spacecraft Systems Develop New GPS Capabilities," *GPS World*, Vol. 13, February 1 2002, pp. 22–31.

[2]J. R. Carpenter, J. A. Leitner, D. C. Folta, and R. D. Burns, "Benchmark Problems for Spacecraft Formation Flying Missions," *AIAA Guidance, Navigation and Control Conference*, Austin, TX, August 11–14 2003. Paper No. AIAA 2003-5364.

[3]L. B. King, G. G. Parker, S. Deshmukh, and J.-H. Chong, "Spacecraft Formation-Flying using Inter-Vehicle Coulomb Forces," tech. rep., NASA/NIAC, January 2002.

[4]L. B. King, G. G. Parker, S. Deshmukh, and J.-H. Chong, "Study of Interspacecraft Coulomb Forces and Implications for Formation Flying," *AIAA Journal of Propulsion and Power*, Vol. 19, May–June 2003, pp. 497–505.

[5]E. G. Mullen, M. S. Gussenhoven, D. A. Hardy, T. A. Aggson, and B. G. Ledley, "SCATHA Survey of High-Voltage Spacecraft Charging in Sunlight," *Journal of the Geophysical Sciences*, Vol. 91, No. A2, 1986, pp. 1474–1490.

[6]E. C. Whipple and R. C. Olsen, "Importance of differential charging for controlling both natural and induced vehicle potentials on ATS-5 and ATS-6," *Proceedings of the 3rd Spacecraft Charging Technology Conference*, Nov. 12–14 1980, p. 887. NASA Conference Publication 2182.

[7]E. Mullen, A. R. Frederickson, G. P. Murphy, K. P. Ray, E. G. Holeman, D. Delorey, R. Robson, and M. Farar, "An Autonomous Charge Control System at Geosynchronous Altitude: Flight Results for Spacecraft Design Considerations," *IEEE Transactions on Nuclear Science*, Vol. 44, December 1997, pp. 2188 – 2914.

[8]J. F. Fennell, H. C. Koons, J. L. Roeder, and J. B. Blake, "Spacecraft Charging: Observations and Relationship to Satellite Anomalies," *Proceedings of 7th Spacecraft Charging Technology Conference*, Noordwijk, The Netherlands, ESA Spec. Publ., April 23–27 2001, pp. 279–285.

[9]H. B. Garrett and A. C. Whittlesey, "Spacecraft Charging, An Update," *IEEE Transactions on Plasma Science*, Vol. 28, Dec. 2000, pp. 2017–2028.

[10]K. Torkar, W. Riedler, F. Rudenauer, C. P. Escoubet, H. Arends, B. T. Narheim, K. Svenes, M. P. McCarthy, G. K. Parks, R. P. Lin, and H. Reme, "Spacecraft Potential Control aboard Equator-S as a Test for Cluster-II," *Annales Geophysicae*, Vol. 17, 1999, pp. 1582–1591.

[11]K. Torkar, W. Riedler, C. P. Escoubet, M. Fehringer, R. Schmidt, G. R. J. L., H. Arends, F. Rudenauer, W. Steiger, B. T. Narheim, K. Svenes, R. Torbert, A. M., A. Fazakerley, R. Goldstein, R. C. Olsen, A. Pedersen, E. Whipple, and H. Zhao, "Active Spacecraft Potential Control for Cluster – Implementation and First Results," *Annales Geophysicae*, Vol. 19, No. 10/12, 2001, pp. 1289–1302.

[12]C. R. Seubert and H. Schaub, "Tethered Coulomb Structures: Prospects and Challenges," *AAS F. Landis Markley Astrodynamics Symposium*, Cambridge, MA, June 30 – July 2 2008. Paper No. AAS 08–269.

[13]K. G. Carpenter, C. J. Schrijver, M. Karovska, and S. M. C. D. Team, "The Stellar Imager (SI) Project: A Deep Space UV/Optical Interferometer (UVOI) to Observe the Universe at 0.1 Milli-arcsec Angular Resolution," *Astrophysics and Space Science*, Vol. 320, April 2009, pp. 217–223.

[14]G. Blackwood, C. Henry, E. Serabyn, S. Dubovitsky, M. Aung, and S. M. Gunter, "Technology and Design of an Infrared Interferometer for the Terrestrial Planet Finder," *AIAA Space 2003*, Long Beach, CA, Sept. 23–25 2003. Paper No. AIAA 2003-6329.

[15]D. P. Scharf, F. Y. Hadaegh, J. A. Keim, A. C. Morfopoulos, A. Ahmed, Y. Brenman, A. Vafaei, J. F. Shields, C. F. Bergh, and P. R. Lawson, "Flight-like Ground Demonstrations of Precision Maeuvers for Spacecraft Formations," *AIAA Guidance, Navigation and Control Conference*, Honolulu, Hawaii, Aug. 18–21 2008. Paper No. AIAA 2008-6665.

Table 3: Summary of the system responses for each test configuration

Test configuration	5% Settling time (s)	Overshoot (%)	Steady state voltage (kV)	Steady state force (mN)	Estimated gravity force (mN)
Nominal	25	$< 15\%$	-	-	-
1. Out-of-plane (starts down)					
Simulation	25	10	-14	2.0	-
Experimental	23	9.0/13.6	-12	1.4	2.0
2. Out-of-plane (starts up)	24	33/48	-15	2.2	2.0
3. Orbit Radial	25	5.3/8.9	± 21.5	2.4	4.5
4. Flat and level	19	3.3/3.3	± 9	0.4	0.0

[16] S.-J. Chung, D. Adams, D. W. Miller, E. Lorenzini, and D. Leisawitz, "SPHERES Tethered Formation Flight Testbed: Advancements in Enabling NASA's SPECS Mission," *SPIE – Proceedings of Astronomical Telescopes and Instrumentation 2006 Conference*, 2006. Paper No. 6268-11.

[17] V. L. Pisacane, *The Space Environment and its Effects on Space Systems*. Reston, VA: AIAA Education Series, 2008.

[18] D. A. Gurnett and B. A., *Introduction to Plasma Physics - with Space and Laboratory Applications*. New York, NY: Cambridge University Press, 2005.

[19] E. C. Whipple, "Potentials of surfaces in space," *Reports on Progress in Physics*, Vol. 44, 1981, pp. 1197–1250.

[20] C. R. Seubert and H. Schaub, "One-Dimensional Testbed for Coulomb Controlled Spacecraft," *AAS/AIAA Spaceflight Mechanics Meeting*, Savannah, GA, Feb. 8–12 2009. Paper No. AAS 09–015.

[21] A. Natarajan and H. Schaub, "Linear Dynamics and Stability Analysis of a Coulomb Tether Formation," *AIAA Journal of Guidance, Control, and Dynamics*, Vol. 29, July–Aug. 2006, pp. 831–839.

[22] J. Berryman and H. Schaub, "Analytical Charge Analysis for 2- and 3-Craft Coulomb Formations," *AIAA Journal of Guidance, Control, and Dynamics*, Vol. 30, Nov.–Dec. 2007, pp. 1701–1710.

[23] J. Berryman and H. Schaub, "Static Equilibrium Configurations in GEO Coulomb Spacecraft Formations," *AAS/AIAA Spaceflight Mechanics Meeting*, Copper Mountain, CO, Jan. 23–27 2005. Paper No. AAS 05–104.

[24] H. Vasavada and H. Schaub, "Analytic Solutions for Equal Mass Four-Craft Static Coulomb Formation," *Journal of the Astronautical Sciences*, Vol. 56, Jan. – Mar. 2008, pp. 7–40.

[25] S. Wang and H. Schaub, "One-Dimensional 3-Craft Coulomb Structure Control," *7th International Conference on Dynamics and Control of Systems and Structures in Space*, Greenwich, London, England, July 16–20 2006, pp. 269–278.

[26] S. Wang and H. Schaub, "1-D Constrained Coulomb Structure Stabilization With Charge Saturation," *AAS/AIAA Astrodynamics Specialist Conference*, Mackinac Island, MI, Aug. 19–23 2007. Paper No. AAS 07–267.

[27] R. D. Robinett, G. G. Parker, H. Schaub, and J. L. Junkins, "Lyapunov Optimal Saturated Control for Nonlinear Systems," *AIAA Journal of Guidance, Control, and Dynamics*, Vol. 20, Nov.–Dec. 1997, pp. 1083–1088.

[28] W. Riedler, K. Torkar, F. Rudenauer, M. Fehringer, A. Pedersen, R. Schmidt, R. J. L. Grard, H. Arends, B. T. Narheim, J. Troim, R. Torbert, R. C. Olsen, E. Whipple, R. Goldstein, N. Valavanoglou, and H. Zhao, "Active Spacecraft Potential Control," *Space Science Reviews*, Vol. 79, Jan. 1997, pp. 271–302.